DEP Particle Dynamics and the Steady Drag Assumption

DEP Particle Dynamics and the Steady Drag Assumption
S.T. Wereley*, I. Whitacre*, R. Bashir** and H.B. Li**

*Purdue University, School of Mechanical Engineering,
West Lafayette, IN 47907-2088, USA, wereley@purdue.edu
**Purdue University, School of Electrical and Computer Engineering,
West Lafayette, IN 47907-2088, USA, bashir@purdue.edu

ABSTRACT

The interaction of fluid drag, dielectrophoretic forces, and Brownian motion on a nanoparticle's motion is studied using a microfluidic chip with interdigitated electrodes. The flow domain is a 11.6 μm deep by 350 μm wide channel with 23 μm wide electrodes located at the bottom surface of the channel and a glass top surface. The electrodes are covered by a thin layer of silicon dioxide to insulate them from the fluid medium, suppressing electrolysis and local Joule heating. Although these phenomena have been considered by other researchers, our experiments and modeling reveal it to be a considerably more complicated phenomenon than previously thought. Using an adapted micro Particle Image Velocimetry technique along with microscopic imaging, particle motion in three-dimensions is measured and compared to predicted results, showing not only the expected horizontal DEP retarding force but also a vertical force away from the electrodes. Further, because of the spatially varying nature of both the DEP force as well as the drag force, one of the main assumptions made in many previous DEP studies must be seriously questioned—whether steady low Reynolds number particle dynamics are insufficient to predict the particle behavior.

Keywords: dielectrophoresis, DEP, PIV, particle, velocity

1 INTRODUCTION AND SET UP

1.1 DEP Device

A dielectrophoretic device has been designed to trap, separate, and concentrate biological components carried in solution. This is done by creating a dielectrophoretic interaction between the spheres and the fluid. The device was designed and manufactured by Haibo Li at Purdue University, a student in Prof. Bashir's research group [1]. The device consists of a microchannel with a depth of 11.6 μm, width of 350 μm, and length of 3.3 mm. The channel was anisotropically etched in silicon to produce a trapezoidal cross-section. The channel was covered by a piece of anodically bonded glass. A schematic view and digital photo of the device are shown in Figure 1. Bright regions represent platinum electrodes and the dark regions represent the electrode gaps. The electrodes are covered by a 0.3 μm thick layer of PECVD silicon dioxide, which insulates the electrodes from the liquid medium, suppressing electrolysis. The electrodes are arranged in interdigitated pairs so that the first and third electrodes from Figure 1 are always at the same potential. The second and fourth electrodes are also at the same potential, but can be at a different potential than the first and third electrodes. An alternating electric potential is applied to the interdigitated electrodes to create an electromagnetic field with steep spatial gradients. Particle motion through the resulting electric field gradients causes polarization of the suspended components, resulting in a body force that repels particle motion into increasing field gradients. In the experiments, sample solutions were injected into the chamber using a syringe pump (World Precision Instruments Inc., SP200i) and a 250μl gas-tight luer-lock syringe (ILS250TLL, World Precision Instruments Inc.). The flow rate could be adjusted and precautions were taken to avoid air bubbles. An HP 33120A arbitrary waveform generator was used as the AC signal source to produce sinusoidal signal with frequency specified at 1MHz.

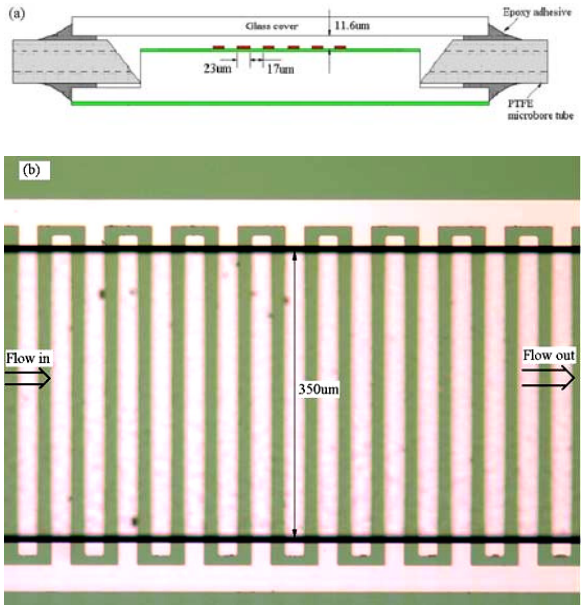

Figure 1. (a) Schematic view of experimental apparatus and (b) photo of apparatus.

1.2 Micro Particle Image Velocimetry

Particle image velocimetry (PIV) is a well accepted technique for acquiring full field velocity information from experimental fluid flows [2]. Micro particle image velocimetry (μPIV) has expanded conventional PIV to utilize microscopic imaging devices as developed by [3]. μPIV results have been used in a number of applications such as a detailed investigation of pressure driven flow through a microchannel [4], micron resolution temperature measurements [5], and investigations of dielectrophoretic particle trapping [6,7].

Figure 2 shows the typical layout of a μPIV system. The measurement volume can be illuminated by either a broad wavelength constant light source or a pulsed laser, such as a frequency doubled Nd:YAG. In these experiments a standard microscope mercury lamp is used. To ensure that all particles have the same properties, 0.7 μm polystyrene latex (PSL) microspheres (Duke Scientific) are suspended in de-ionized water in dilute concentrations (less than 0.1% by volume). Tracer particles in the measurement volume are coated with a red fluorescing dye (λ_{emit}=542 nm, λ_{emit}=612 nm). Images are captured with precise time delay separating exposures. The image sets are then divided into interrogation regions. The corresponding interrogation regions from consecutive images are cross-correlated to determine the most likely relative displacement of the particles in the interrogation regions in the form of a cross-correlation peak. Reducing the size of an interrogation region reduces the measurement volume and increases the spatial resolution of a measurement so long as displacements are less than half the size of an interrogation region, i.e. the Nyquist criterion.

The images were acquired using a Photometrics CoolSNAP HQ interline transfer monochrome camera (Roper Scientific). This camera is capable of 65% quantum efficiency around the 610 nm wavelength. The largest available image size that can be accommodated by the CCD array is 1392 by 1040 pixels, but the camera has the capability of pixel binning, which can drastically increase the acquisition frame rate by reducing the number of pixels that need to be digitized. A three-by-three pixel binning scheme was used in this experiment, producing images measuring 464 by 346 pixels, which were captured at a speed of 20 frames per second. The average focused particle diameter in the images was approximately 3 pixels.

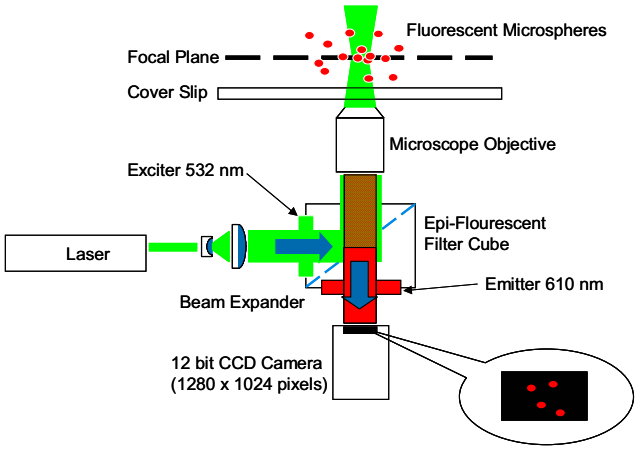

Figure 2. Diagram of typical μPIV system.

Shallow Channel Considerations

When performing μPIV measurements on shallow microchannels, the depth of focus of the microscope can be comparable in size to the depth of the flow. A PIV cross-correlation peak, the location of which is the basis for PIV velocity measurements, is a combination of the velocity distribution in the interrogation region and some function of average particle shape. PIV velocity measurements containing velocity gradients can substantially deviate from the ideal case of depthwise uniform flow. Gradients in the in-plane direction have been addressed by image correction techniques [8], but gradients in the depthwise direction remain problematic. They can cause inaccurate velocity measurements due to the presence of multiple velocities within an interrogation region that are independent of mesh refinement. One problem with depthwise velocity gradients is cross-correlation peak deformation which reduces the signal to noise ratio of a PIV measurement [9]. Cross-correlation peak deformation can also reduce the effectiveness of subpixel peak fitting schemes which are based on a particular cross-correlation shape, such as a common five point Gaussian fit.

2 EXPERIMENTAL RESULTS

The experiments presented here designed to quantify the dielectrophoretic performance of the device. The experiments used six sets of 800 images each to analyze the effect of dielectrophoresis on particle motion in the test device. These images are high quality with low readout noise, as can be seen in the example fluorescent image of Figure 3. The top image demonstrates the many different particle intensity distributions which are typically present in a μPIV image in which the particles are distributed randomly within the focal plane. The bottom figure shows how, as the result of the DEP force, the particles migrate to the top of the channel and all have nearly identical images. The top image also shows that when a significant DEP force exists, the particles are trapped at the electrode locations by the increase in DEP force there. In general, the observed particle image shape is the convolution of the geometric particle image with the point response function of the imaging system. The point response function of a microscope is an Airy function when the point being imaged is located at the focal plane. When the point is displaced from the focal plane, the Airy function becomes a Lommel function [10]. Both Airy and Lommel functions feature concentric rings, although at different intensities

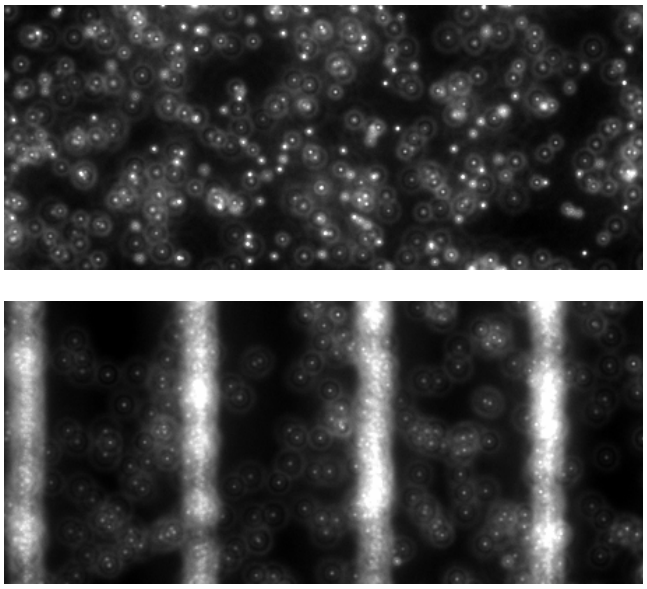

Figure 3. A photo of PSL particles with 0.0 volts (top) and 4.0 volts (bottom).

and diameters. For a standard microscope the diffraction limited spot size is given by

$$d_e = \frac{1.22 \cdot \lambda}{NA} \qquad (1)$$

A numerical aperture (or NA) of 1.00 and an incident light wavelength λ of 540nm results in a diffraction limited spot size of 0.66μm, while the particles used are 0.69μm. Consequently the particle intensity distributions as recorded by the camera are partly due to the geometric image of the particle and partly due to diffraction effects. Hence, the distance of any particle from the focal plane can be determined by the size and shape of the diffraction rings.

A conventional μPIV analysis was performed to obtain an initial estimate of the average particle velocity field. Because the goal of the conventional μPIV analysis is not to extract velocity distribution, only the median velocity is reported. The spatial resolution can be higher than when using a velocity distribution analysis method such as the synthetic image method. In section 5.4, the velocity field will be extracted using the synthetic image approach. The PIV images were analyzed with *EDPIV*[1], an advanced μPIV interrogation package written in part at Purdue University by Lichuan Gui. An interrogation region of 32 by 32 pixels and a grid spacing of 8 by 8 pixels were used. Figure 4 shows vector plots for the experimental cases of 0.5 volts (top) and 4.0 volts (bottom). A uniform color scale was applied to these figures for representing velocity magnitude, such that velocity changes between cases can be

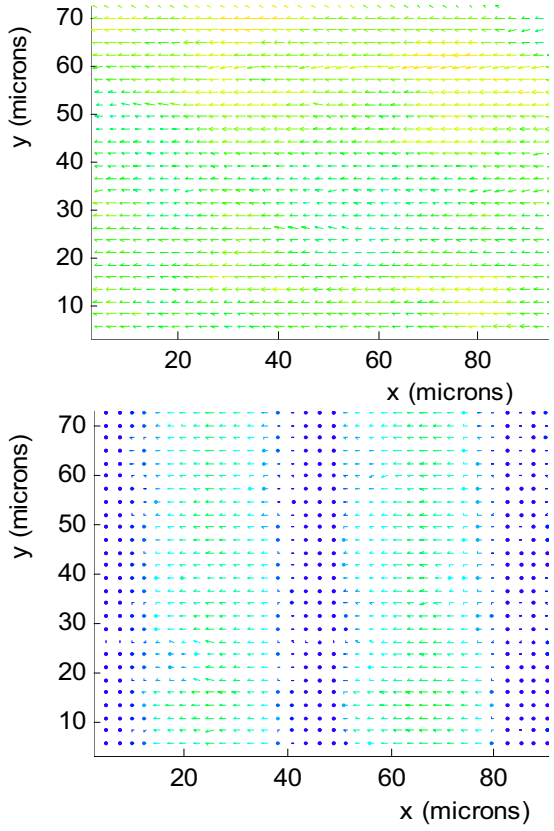

Figure 4. PIV vector plots for electrode voltages of 0.5 volts (top) and 4.0 volts (bottom).

more easily interpreted. In all cases, the electrode voltage signal frequency was set to 580 kHz. This was determined by sweeping between frequencies of 100 kHz to 10MHz and qualitatively determining the most effective trapping frequency.

The PIV results are summarized in Figure 5 which shows the average axial velocities for the six electrode

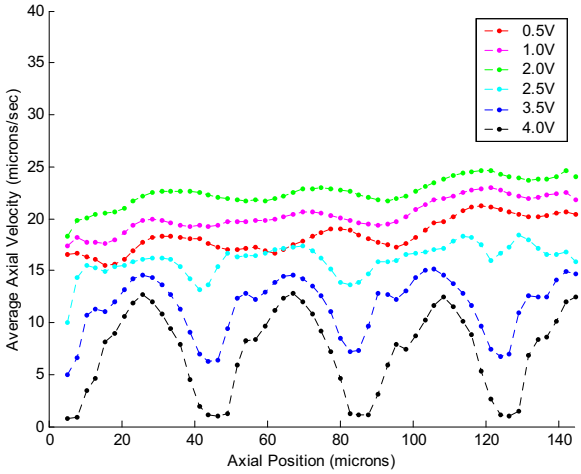

Figure 5. Average axial velocity from PIV results for all electrode voltage cases.

[1] Evaluation version available at http://www.ecn.purdue.edu/microfluidics/Edpiv.zip

voltage cases. The three lowest voltages share a trend of decreasing particle velocity in the downstream direction. This phenomenon is evident in the average velocity curves in Figure 5. One explanation for this behavior may be that with each electrode a particle encounters, it lags the fluid velocity a little more. The cumulative effect results in a gradual slowing of the particle.

Another interesting result apparent from Figure 5 is that initially the average particle velocity increases as the voltage increases, 0.5 volts to 2.0 volts. This phenomenon is explained by particles being displaced from the channel bottom into faster areas of the fluid flow. This biases the velocity distribution toward higher velocities, altering the shape of the cross-correlation peak to favor higher velocities even though the fluid flow is constant. For higher voltages the effect of particles being hindered by axial field gradients is compounded by particles being forced beyond the high speed central portion of the flow profile by the DEP force. It can be qualitatively confirmed that particles migrate to the top of the channel by observing particle shapes in the images from the higher voltage cases, i.e. comparing the many particle shapes found in Figure 3 (top) which is acquired at 0.5 volts with the single particle shape found in Figure 3 (bottom) which is acquired at 4.0 volts. It is confirmed that the particles are indeed at the top of the channel by traversing the focal plane throughout the depth of the device.

The experimental results in Figure 5 were fit to the simple phenomenological model

$$V_{axial} = A \cdot x + B + C \cdot \sin\left(2\pi / D + E\right) \qquad (2)$$

by minimizing the root mean square difference between the fit function and the experimental data. The resulting constants capture important dynamics of the particle velocity. The *A* coefficient captures particles speeding up or slowing down as they pass through the device. The *B* coefficient captures the mean velocity of the particles within the device and the *C* coefficient captures the sinusoidal behavior of particles as they encounter each electrode. These results are shown graphically in Figure 6. The parameters for the cases of 0.5 to volts 2.5 volts are very similar, with the exception of a gradual increase in *B*. In the two highest voltage cases the linear slope *A* is reduced to nearly zero indicating that the particles do not speed up or slow down as they pass through the devices while the magnitude of the sinusoidal component *C* is greatly increased. From these results it is apparent that the particle velocities are reduced as particles travel downstream for low electrode voltages, and that the particles are dominated by a periodic trajectory for higher electrode voltages.

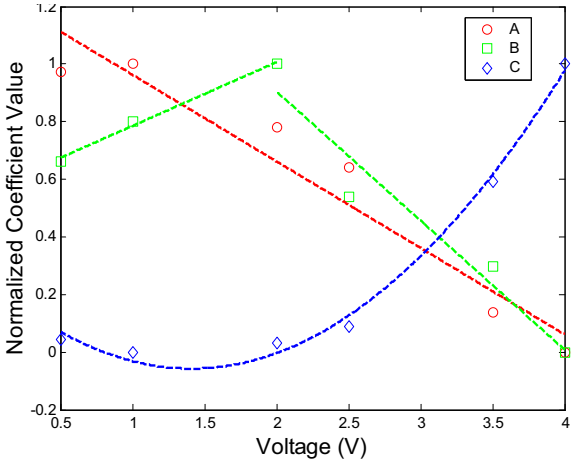

Figure 5. Curve fit parameters from Eq. 2 versus electrode voltage. The dashed lines represent linear, piecewise linear, and parabolic curve fits for parameters *A*, *B*, and *C*.

3 CONCLUSIONS

The dynamics of particles traveling through the device described in this paper are very complicated, exhibiting migration normal to the electrodes as well as trapping behavior in the plane of the electrode. Further work is needed to assess the accuracy of the steady drag assumption.

REFERENCES

[1] HB Li, Y Zheng, D Akin, R Bashir, "Characterization and Modeling of a Micro-Fluidic Dielectrophoresis Filter for Biological Species," *submitted* to J. Microelectromechanical Sys. (2004).

[2] R.J. Adrian, "Particle-imaging techniques for experimental fluid mechanics," Ann. Rev. Fluid Mech., Vol. 23, 261-304, 1991.

[3] J.G. Santiago, S.T. Wereley, C.D. Meinhart, D.J. Beebe, R.J. Adrian, "A particle image velocimetry system for microfluidics," Experiments in Fluids, Vol. 25, 316-319, 1998.

[4] C.D. Meinhart, S.T. Wereley, J.G. Santiago, "PIV measurements of a microchannel flow," Experiments in Fluids, Vol. 27, 414-419, 1999.

[5] V. Hohreiter, S.T. Wereley, M. Olsen, and J.Chung, "Cross-correlation analysis for temperature measurement," Meas. Sci. Tech., Vol. 13, 1072-1078, 2002.

[6] E.B. Cummings, "A comparison of theoretical and experimental electrokinetic and dielectrokinetic flow fields," AIAA 2002-3193, 2002.

[7] C.D. Meinhart, D. Wang, K. Turner, "Measurement of Ac Electrokinetic Flows," Biomedical Microdevices, Vol. 5, No. 2, 139-145, 2002.

[8] S.T. Wereley, L. Gui, C.D. Meinhart, "Advanced Algorithms for Microscale Velocimetry," AIAA J., Vol. 40, No. 6, 1047-1055, 2002.

[9] E.B. Cummings, "An image processing and optimal nonlinear filtering technique for PIV of microflows", Experiments in Fluids, Vol. 29, [Suppl.]:S42-50, 2001.

[10] M. Born, E. Wolf, Principles of optics, Oxford Press, Pergamon, 1997.